

Spontaneous Motion of Liquid Droplets on Soft Gradient Surfaces

Weiwei Zhao,¹ Wenjie Qian,¹ and Qin Xu^{1,*}

¹*Department of Physics, The Hong Kong University of Science and Technology, Hong Kong, China*
(Dated: July 16, 2024)

We report an experimental investigation of the spontaneous motion of liquid droplets on soft gels with a crosslinking gradient. By systematically adjusting the spatial difference in crosslinking density, we observed that millimeter-sized liquid droplets moved along the gradient of elastic modulus and even climbed tilted slopes against gravity. Unlike the wetting dynamics of micro-droplets, which are governed by elastocapillary effects, we demonstrated that the observed spontaneous movements of millimeter-sized droplets were attributed to the surface energy difference resulting from the variation in crosslinking density. Using *in-situ* confocal microscopy imaging, we analyzed the viscoelastic dissipation induced by the moving wetting ridges near dynamic contact lines. Based on the relationship between the crosslinking density and surface energy of soft gels, our findings reveal a new method for controlling droplet dynamics at soft and dissipative interfaces.

The dynamic wetting of droplets on soft interfaces plays a crucial role in various biological processes and engineering applications, including the mechanosensing of cells [1], tissue growth on soft substrates [2], microfluidic device design [3], and micro-scale drug delivery [4]. Moreover, moving liquid droplets have been used as probes to characterize the tribology and interfacial rheology of soft interfaces [5–7]. Therefore, a precise control of droplet motion on soft surfaces is highly desirable from both scientific and engineering perspectives.

However, the manipulation of droplet dynamics on compliant surfaces has been much less studied compared with that on rigid substrates [8–11]. It is highly challenging to use traditional methods, such as chemical deposition and surface roughness patterning [12, 13], to modify the surface energy of soft surfaces due to the presence of diffusive solvents and solid capillarity. Consequently, while theoretical modelling have been employed to predict the droplet motion on soft gradient surfaces [14–16], there has been little direct experimental validation of these predictions. Previous research showed that micro-droplets can spontaneously move along thickness gradient on soft gels due to elastocapillary effects [17]. However, this spontaneous movement occurs only when the droplet sizes are as small as the elastocapillary length of the substrates, typically on the order of 10 μm .

In this work, we report an experimental observation of the spontaneous motion of millimeter-sized droplets on soft gel surfaces with a sharp gradient in crosslinking density. By combining the measurements of dynamic contact angles and confocal imaging of moving contact ridges, we demonstrated that the difference in crosslinking density leads to variations in the surface energy of soft gels. The resulting imbalance in contact forces can cause large liquid droplets to move spontaneously, thereby counterbalancing the viscoelastic dissipation from substrates and even overcoming gravity along a tilted surface.

I. EXPERIMENTAL SYSTEM

We prepared the soft substrates by mixing polydimethylsiloxane (PDMS) polymers (Gelest, DMS-V31) with dimethylsiloxane copolymer crosslinkers (Gelest, HMS-301). The resulting mixtures were cured into soft silicone gels at 40°C for 24 hours. The elasticity of these gels was quantitatively controlled by the weight ratio of the crosslinkers (k) [18]. By systematically varying the crosslinking density from $k = 0.67\%$ to 5.0 %, the Young's moduli of the cured gels ranged between $E = 0.16$ kPa and 175 kPa.

To create a soft gradient surface, we first fabricated a stiff gel film with a surface area of 5 cm \times 5 cm and a thickness of $h = 500$ μm . By maintaining $k \geq 2.5\%$, we kept the Young's modulus of the stiff film in the range of $E_2 > 80$ kPa. We then cut out a 2 cm \times 1 cm rectangular piece from the center of the gel film, filled this rectangular hole with a PDMS mixture containing a low density of crosslinkers ($k \leq 1.0\%$), and cured the filled gel film. The resulting substrate comprised a soft region with a Young's modulus of $E_1 < 6$ kPa was surrounded by a stiff region. To ensure that the entire substrate was flat, we precisely controlled the amount of added PDMS mixture by monitoring the interface between the soft and stiff regions using a high-resolution digital camera. Due to swelling effects, there was inevitably a 5 μm deformed region near the boundary between soft and stiff gels (Supplemental Fig. S1). Nevertheless, throughout all our experiments, these boundary defects have remained substantially smaller than the sizes of droplets.

The droplets were composed of an aqueous mixture comprising 80 % glycerol and 20 % water, with an effective viscosity of $\eta = 43$ cSt. As illustrated in Fig. 1(a), we initially placed a liquid droplet with a diameter of $D \sim 3.5$ mm on the boundary between the soft and stiff gels ($t = 0$ s). By using two digital cameras, we simultaneously captured the side and bottom views of the droplet movements at $t > 0$ s. The effective surface tension of these aqueous droplets on silicone gels was measured using the sessile droplet method [18] and found to

* qinxu@ust.hk

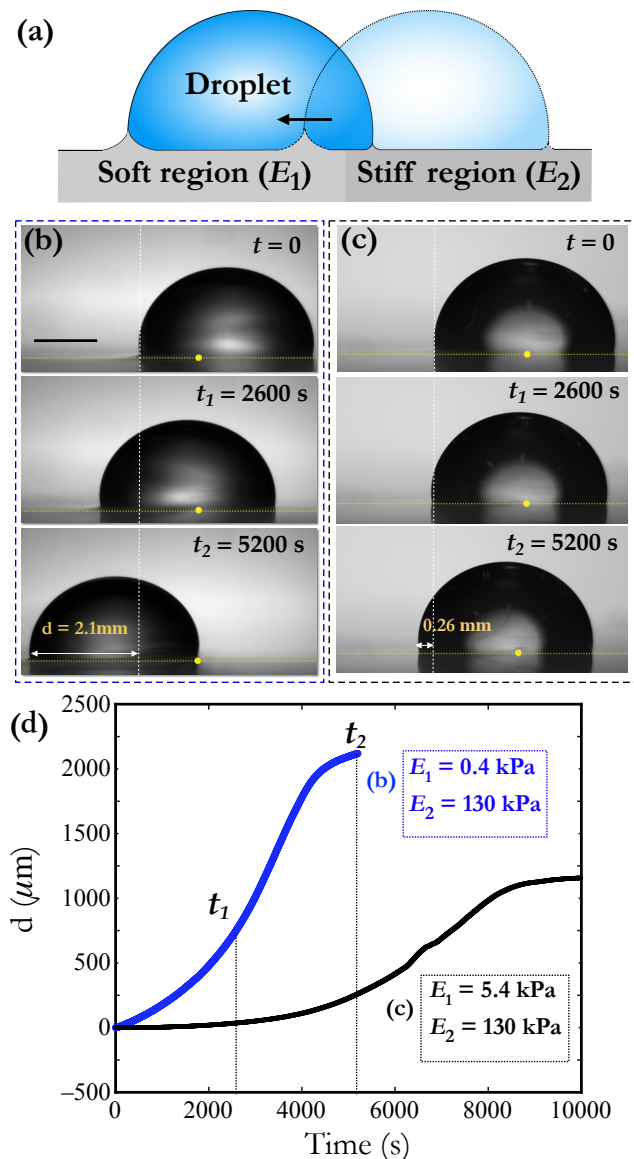


FIG. 1. **Droplet migration on soft gradient substrates.** (a) Schematic illustration of a droplet moving from a stiff region (E_2) to a soft region (E_1) along a substrate. (b) Snapshots of a moving droplet at different times, $t = 0$ s, $t_1 = 2600$ s, and $t_2 = 5200$ s. The Young's moduli of the soft and stiff regions were $E_1 = 0.4$ kPa and $E_2 = 130$ kPa, respectively. (c) A moving droplet on a soft gradient substrate with $E_1 = 5.4$ kPa and $E_2 = 130$ kPa. (d) Plots of droplet displacement (d) against time for the two droplets shown in the panels (b) and (c), respectively.

be $\gamma_l = 42$ mN/m. This value is significantly less than the surface tension of pure glycerol (~ 69 mN/m) due to the extraction of free chains at contact lines [19].

Figures 1(b) and (c) depict the spontaneous movements of an aqueous droplet on the substrates with different combinations of E_1 and E_2 . The white solid dots in the snapshots indicate the boundaries between gels. In both cases, the stiff regions had a constant $E_2 = 130$ kPa,

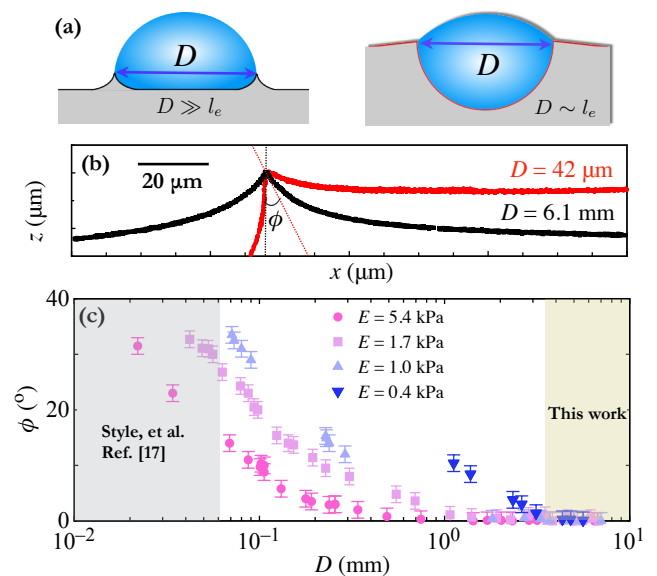


FIG. 2. **Role of elastocapillarity.** (a) Schematics illustrating the rotation of the liquid–air contact line when the droplet diameter (D) is close to the elastocapillary length (l_e). (b) The red and black curves represent the wetting profiles induced by droplets with $D = 42$ μm and $D = 6.1$ mm, respectively, on a soft gel with $E = 1.7$ kPa. The elastocapillary length (l_e) was approximately 10 μm. The rotational angle (ϕ) was determined by comparing the two profiles. (c) Plots of ϕ against D for $E = 5.4$ kPa, $E = 1.7$ kPa, $E = 1.0$ kPa and $E = 0.4$ kPa. The shaded gray and brown–gray areas indicate the droplet sizes investigated in ref. [17] and this study, respectively.

while the Young's moduli of soft regions varied from $E_1 = 0.4$ kPa in panel (b) to $E_1 = 5.4$ kPa in panel (c). The droplets on both substrates spontaneously moved along the gradient of crosslinking density, with the difference between E_1 and E_2 playing a crucial role in determining the moving speed. For instance, within 5200 s, the droplet in Fig. 1(b) moved a distance of 2.1 mm, while the droplet in (c) moved only 0.26 mm. The plots of displacement d against time for these two droplets are presented in Fig. 1(d), which clearly demonstrate the influence of the crosslinking gradient on the droplet motion.

II. ROLE OF ELASTOCAPILLARITY

We first examined whether the elastocapillary effects of soft substrates were essential for the droplet movements that we observed. This effect is characterized by the elastocapillary length, $l_e = \Upsilon_s/E$, where Υ_s is the surface stress of a soft substrate, respectively [20]. As shown in the schematic in Fig. 2(a), when the droplet diameter is close to the elasto-capillary length, $D \sim l_e$, the contact line rotates by an angle ϕ relative to the non-rotating contact line of a large droplet, $D \gg l_e$ [20]. Given that ϕ depends on the substrate thickness, a previous study

from Style et al. [17] showed that micro-droplets ($D \sim l_e$) spontaneously moved along soft substrates with a thickness gradient. In the present work, as the droplets were several millimeters in size, it is unlikely that the elastocapillary effects were still crucial to the droplet movements. To confirm this assumption, we performed confocal imaging of static wetting profiles on soft gels with uniform Young's moduli ranging from $E = 0.4$ kPa to 5.4 kPa. By depositing a layer of 200 nm fluorescent particles at soft interfaces, we obtained the wetting profiles using a particle locating method [21]. For example, Fig. 2(b) shows the obtained wetting profiles induced by droplets with sizes of $D = 41 \mu\text{m}$ and $D = 6 \text{ mm}$, respectively, on the same soft gel with $E = 1.7$ kPa. As l_e was approximately $15 \mu\text{m}$, we observed an apparent rotation of the wetting ridge for the smaller droplet ($D = 41 \mu\text{m}$). The rotational angle ϕ of the contact line was quantitatively determined by comparing the two ridge profiles.

Figure 2(c) shows the plots of ϕ against D on soft gels with different Young's moduli ($E = 0.45$ kPa, 0.7 kPa, 1.5 kPa, and 5.4 kPa) and a constant sample thickness of $h = 500 \mu\text{m}$. For each E , ϕ initially decreased with D until it became negligible for large droplets. The critical droplet size that marked the crossover between the two regimes was characterized by $l_e = \Upsilon_s/E$ and therefore decreased with E . Across all the tested substrates, we consistently observed that $\phi \approx 0^\circ$ as $D > 3.3 \text{ mm}$. Hence, for the millimeter-sized droplets in this study, we conclude that elastocapillarity played an insignificant role in driving the movements of the millimeter-sized droplets examined in this study.

III. DRIVING FORCES ON A MOVING DROPLET

To understand the underlying mechanisms of the spontaneous droplet motion, we further measured the macroscopic shapes of a moving droplet. In Fig. 3(a), snapshots from a bottom view show a liquid droplet moving from a stiff region ($E_2 = 130$ kPa) to a soft region ($E_1 = 0.4$ kPa) over a 5200 s period. The center of this droplet was positioned in the stiff region at $t = 0$ s. Subsequently, the droplet started moving towards the soft region and eventually came to a stop after crossing the boundary between the two regions at $t = 5200$ s. Figure 3(b) shows the changes in the velocity (V) and acceleration (a) of the center of the droplet over time. The peaks of V and a occurred at similar times, indicating significant dissipation force acting on the moving droplet.

We also characterized the width (w) of the droplet intersecting with the boundary between the two gels. Figure 3(c) shows the plot of w against time, where the maximum width corresponds to the droplet diameter, $w_m = D$. By comparing the plots in Figs. 3(b) and (c), we observed that both a and w reached their maximum values simultaneously. To validate the generality of this observation, we systematically varied both the droplet

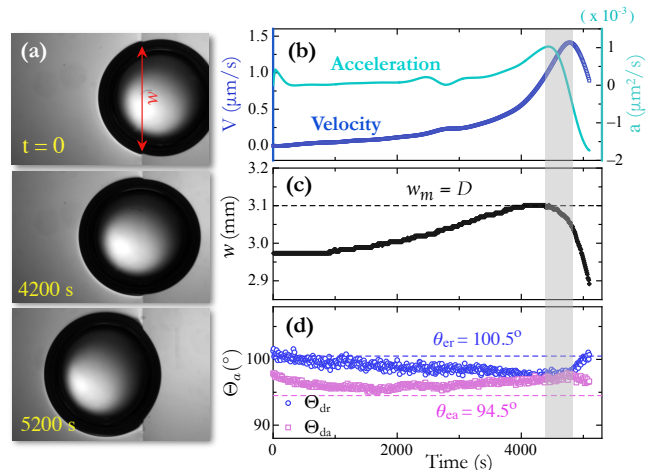


FIG. 3. **Dynamics of the moving droplets.** (a) Bottom view snapshots of a moving droplet at $t = 0$ s, 4200 s, and 5200 s, respectively. The soft region (left) and the stiff region (right) had the Young's moduli of $E_1 = 0.4$ kPa and $E_2 = 130$ kPa, respectively. The red line with arrows indicates the width w . (b) Plots of velocity (V) and acceleration (a) against time for the droplet in (a). (c) Plot of w against time. (d) Plots of the advancing dynamic contact angle Θ_{da} (open blue circles) and receding dynamic contact angle Θ_{dr} (pink open squares) against time. The blue and pink dashed lines indicate the equilibrium contact angles in the advancing (θ_{ea}) and receding directions (θ_{er}), respectively. The gray region across (b)-(d) indicates a period when the acceleration (a) and the velocity (V) of the droplet reach their peaks almost simultaneously. Within this period, we observed that $w = D$ and $\Theta_{dr} = \Theta_{da}$.

sizes (D) and the difference in the Young's moduli between the two gels (E_1 and E_2). Across all our measurements, the peak values of a and w were synchronized in time (Supplemental Fig. S2). This result indicates that the maximum force propelling a droplet consistently occurs when the center of the droplet reaches the boundary between the two gels.

Here, we consider the contact forces acting on the dynamic contact lines. At the advancing contact line of a moving droplet, the net lateral capillary force is given by

$$F_a = \kappa\gamma lw(\cos\theta_{ea} - \cos\Theta_{da}), \quad (1)$$

where θ_{ea} and Θ_{da} are the static and dynamic contact angles on the soft regions, respectively; and $\kappa \approx 1$ is a geometrical constant [6, 22]. Similarly, the lateral capillary force at the receding contact line can be written as

$$F_r = \kappa\gamma lw(\cos\Theta_{dr} - \cos\theta_{er}), \quad (2)$$

where θ_{er} and Θ_{dr} are the static and dynamic contact angles on the stiff regions, respectively. Therefore, the

net contact force acting on the droplet becomes

$$F_d = F_a + F_r = \kappa\gamma_l\omega[(\cos\Theta_{dr} - \cos\Theta_{da}) + (\cos\theta_{ea} - \cos\theta_{er})]. \quad (3)$$

In Eq. 3, the term in the first parenthesis represents the difference between the advancing and receding contact angles (Θ_{da} and Θ_{dr}), while the term in the second parenthesis represents the difference between the equilibrium contact angles on soft and stiff gels (θ_{ea} and θ_{ra}).

To estimate F_d , we measured the dynamic contact angles using a side camera. Figure 3(d) shows the plots of Θ_{da} (red dots) and Θ_{dr} (blue circles) against time for the droplet shown in (a), with the solid red line and blue dashed line representing the equilibrium contact angles, $\theta_{ea} = 94.5^\circ$ and $\theta_{er} = 100.6^\circ$, respectively. Throughout the measurement period, $\theta_{ea} \leq \theta_{da}$ and $\theta_{er} \geq \theta_{dr}$ consistently, and thus both contact forces F_a and F_r remained positive during the droplet movement. At the boundary ($w = D$), we found that $\Theta_{da} \approx \Theta_{da} \approx 97.5^\circ$. Hence, Eq. 3 gives the maximum driving force

$$F_{dmax} = \kappa\gamma_l D(\cos\theta_{ea} - \cos\theta_{er}). \quad (4)$$

As $\Theta_{da} \approx \Theta_{ra}$ when $w = D$ in all the measurements (Supplemental Fig. S3), we concluded that F_{dmax} was solely governed by the difference in equilibrium contact angles between the two gels (θ_{ea} and θ_{er}).

To relate θ_{ea} and θ_{er} to the droplet dynamics, we systematically varied the combination of E_1 and E_2 . Figure 4(a) shows the equilibrium contact angle (θ_e) of a 6-mm static droplet sitting on silicone gels with a constant thickness $h = 500 \mu\text{m}$ but different Young's moduli (E). Considering the negligible influence of elastocapillarity on the contact angles of these large droplets, the plot indicates a decrease in surface energy of silicone gels with the reduction of crosslinking density. We focused on the ranges of E_1 and E_2 that are indicated by the two gray-shaded regions in the figure. We found that a minimum difference in the equilibrium contact angle $\Delta\theta_c = \theta_{er} - \theta_{ea} = 1.2^\circ$ was necessary to initiate spontaneous droplet motion.

To illustrate the tendency of these spontaneous movements, we analyzed how droplets climbed tilted surfaces against gravity. Figure 4(b) exhibits the steepest slopes, characterized by a tilted angle β_m , for a droplet to climb spontaneously with different selections of E_1 and E_2 . For $E_1 = 5.4 \text{ kPa}$ and $E_2 = 99 \text{ kPa}$, $\theta_{er} - \theta_{ea}$ is approximately 1.2° , which equals $\Delta\theta_c$ (green circles in Fig. 4(a)). Within experimental uncertainties, a 3.5-mm droplet could move only on a level substrate ($\beta_m = 0^\circ$). For $E_1 = 1.7 \text{ kPa}$ and $E_2 = 130 \text{ kPa}$, $\theta_{er} - \theta_{ea} \approx 1.8^\circ > \Delta\theta_c$, allowing a droplet to spontaneously climb a tilted plane with a maximum angle of $\beta_m = 3.0^\circ \pm 0.5^\circ$. By further increasing the stiffness gradient by using $E_1 = 0.4 \text{ kPa}$ and $E_2 = 175 \text{ kPa}$, the difference in equilibrium contact angle became as large as $\theta_{er} - \theta_{ea} \approx 5.2^\circ > \Delta\theta_c$. Consequently, a droplet of the same size moved on a slope

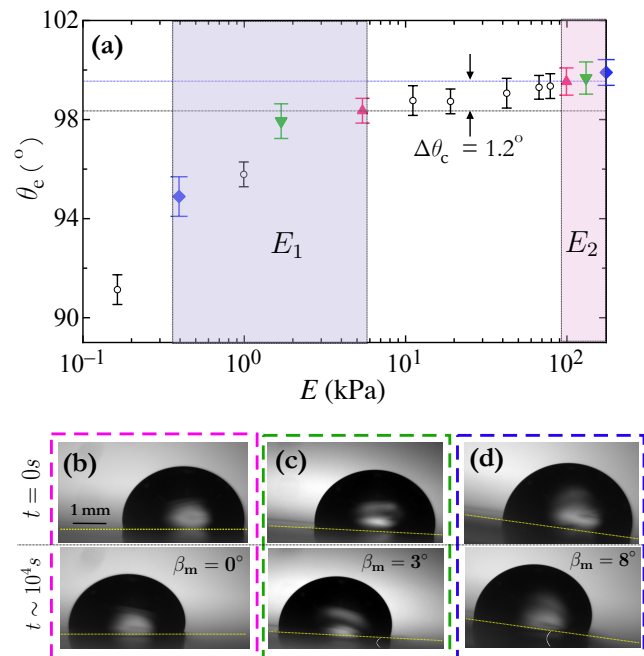


FIG. 4. **Spontaneous motion of droplets against gravity.** (a) Plot of the equilibrium contact angle (θ_e) of a 6-mm static droplet against the Young's modulus of the substrate (E). The substrate thickness is consistently $h = 500 \mu\text{m}$. The two shaded areas represent the range of selected E_1 and E_2 , respectively. The paired data points with different colors (red up-triangles, green down-triangles, and blue diamonds) indicate the selected E_1 and E_2 of the substrates, droplet movements on which are presented in the following panels. (b) With $E_1 = 5.4 \text{ kPa}$ and $E_2 = 99 \text{ kPa}$, a 3.5-mm droplet can only move on a level substrate ($\beta_m = 0^\circ$). (c) With $E_1 = 1.7 \text{ kPa}$ and $E_2 = 130 \text{ kPa}$, a 3.5-mm droplet can climb a plane with a maximum tilted angle of $\beta_m = 3^\circ$. (d) With $E_1 = 0.4 \text{ kPa}$ and $E_2 = 175 \text{ kPa}$, a 3.5-mm droplet can climb a plane with a maximum tilted angle of $\beta_m = 8^\circ$. The yellow dotted lines represent the surfaces of the slopes.

with $\beta_m = 8.0^\circ \pm 0.6^\circ$. Thus, the behavior exhibited in Fig. 4(b) demonstrates how the difference between θ_{ea} and θ_{er} controlled the spontaneous motion of droplets, as indicated by Eq. 4.

IV. DISSIPATION FROM THE SUBSTRATES

As the droplets consistently stopped shortly after crossing the boundary between the soft and stiff regions of the substrate, we expect significant dissipations from the substrates. We first explored the viscoelastic contribution from the moving wetting ridges at contact lines [23–25]. The rheology of soft silicone gels is well described by the Chasset-Thrion model [18], as follows:

$$G^*(\omega) = G'(\omega) + iG''(\omega) = G_0[1 + (i\omega\tau_c)^n], \quad (5)$$

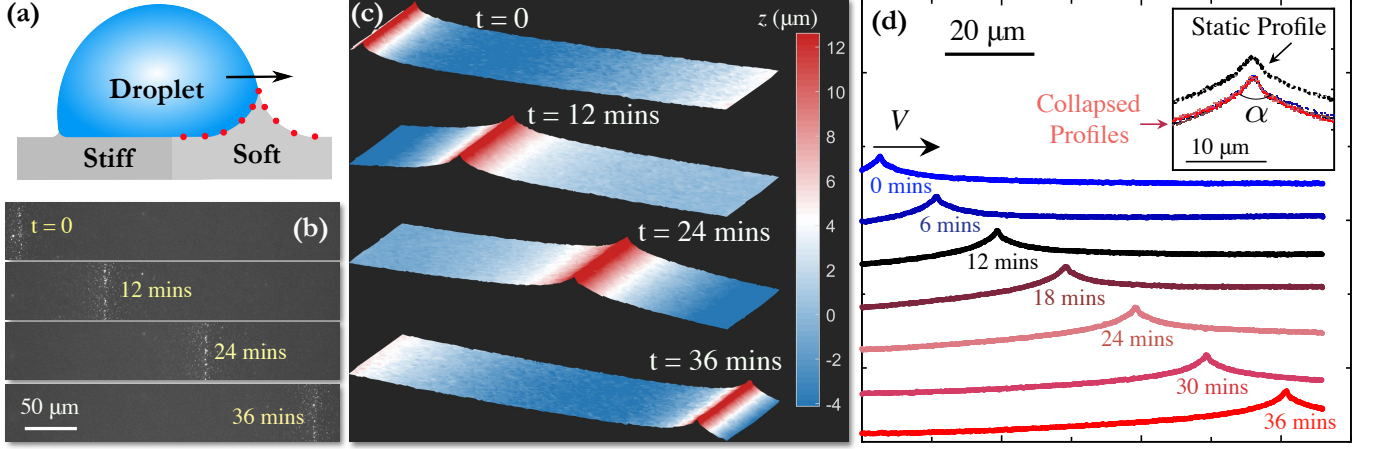


FIG. 5. **Profiles of a moving contact ridge.** (a) Schematic illustration of the confocal microscopy that was used to measure the moving contact profile in the advancing direction. The red dots represent the 200-nm fluorescent nano-beads. (b) Fluorescence images of a contact line advancing along a substrate with $E_1 = 5.4$ kPa and $E_2 = 130$ kPa. (c) Reconstructed three-dimensional (3D) images of the advancing contact ridge (on the soft region with $E_1 = 5.4$ kPa) at $t = 0$ min, 12 min, 24 min, and 36 min. (d) Two-dimensional (2D) plots of the advancing contact ridge at different times. The plots are shifted vertically for visualization. Inset: The profiles shown in (d) collapsed near the contact point and compared with the static wetting profile (the black dots) measured on soft gels with $E = 5.4$ kPa.

where G_0 is the linear shear modulus at zero frequency, and τ_c is a characteristic relaxation timescale. In a quasi-static regime ($V \ll \gamma_l / (G_0 \tau_c)$) [24], the dissipative force resulting from a moving contact ridge can be estimated as [25]

$$F_{dis} \approx \Upsilon_s w \left(\frac{\tau_c G_0 V}{\Upsilon_s} \right)^n \left(\frac{\gamma_l}{\Upsilon_s} \sin \Theta \right)^2, \quad (6)$$

where Θ is the moving contact angle.

To assess the quasi-static condition assumed in Eq. 6, we employed confocal microscopy again to image a moving contact ridge in the advancing direction within the soft region. Conversely, the contact ridges within the stiff region ($E_2 > 80$ kPa) were significantly smaller than $1 \mu\text{m}$, making them challenging to resolve through confocal microscopy. Figure 5(b) shows the fluorescence images of an advancing contact line on a soft region with $E_1 = 5.4$ kPa, while the Young's modulus of the stiff region was $E_2 = 130$ kPa. A particle tracking method was used to obtain the reconstructed moving ridges, as shown in Fig. 5(c). Due to the azimuthal symmetry, the moving ridge profiles were further collapsed to two-dimensional plots, as depicted in Fig. 5(d). The moving speed of the droplet has been limited to the order of $V \sim 10^{-1} \mu\text{m/s}$, which was significantly lower than the critical speed $\gamma_l / (G_0 \tau_c) \sim 10 \mu\text{m/s}$ of the soft region (Supplemental Fig. S4). Therefore, we assumed that the quasi-static assumption of Eq. 6 remained valid. The inset in panel (d) further verifies that the local geometry of the moving ridge remained consistent with the static profile, featuring a constant opening angle of $\alpha = 68^\circ \pm 1.3^\circ$. By considering the local stress balance determined by the Neumann triangle [20], we obtained the surface stress of the soft region, $\Upsilon_s = 2\gamma_l / \cos(\alpha/2) = 25.3$ mN/m.

We quantitatively compared the maximum driving force F_{dmax} with the dissipative force F_{dis} . With $D = 3.2$ mm for the droplet shown in Fig. 5, we obtained $F_{dmax} \approx 5.8 \mu\text{N}$ from Eq. 4. Furthermore, the viscoelasticity of the soft region was fitted to the Chasset–Thirion model with $G_0 = 1.7$ kPa, $n = 0.63$, and $\tau_c = 13$ ms. As the maximum moving speed was less than $0.5 \mu\text{m/s}$, we estimated from Eq. 6 that the dissipative force at the advancing contact line was $F_{dis1} \leq 1.6 \mu\text{N}$.

As the wetting ridges on the stiff region were too small to be imaged by confocal microscopy, we only estimated the upper bound of the dissipative force in the receding direction. A previous work has shown that the surface stress of silicone gels increases with crosslinking density, and that $\Upsilon_s = 30$ mN/m for $E = 14$ kPa [18]. Hence, for the stiff region with $E_2 = 130$ kPa, we expect that $\Upsilon_s > 30$ mN/m. Moreover, fitting the complex moduli of silicone gels to the Chasset–Thirion model becomes challenging for $E_2 > 80$ kPa due to a short relaxation time scale, $\tau_c < 3$ ms. By varying the crosslinking density (k), we found that $G_0 \tau_c$ first decreased with k for $k < 0.9\%$, and then asymptotically approached $G_0 \tau_c \sim 20$ Pa-s when $k > 0.9\%$ (Supplemental Fig. S4). Hence, we expect that $G_0 \tau_c \leq 20$ Pa-s for $E_2 = 130$ kPa. By using $\Upsilon_s = 30$ mN/m and $G_0 \tau_c = 20$ Pa-s, we estimated the upper bound of the dissipative force at the receding contact line as $F_{diss2} < 1.4 \mu\text{N}$ from Eq. 6. Consequently, the total dissipative force induced by the moving wetting ridges, $F_{diss} = F_{diss1} + F_{diss2} < 3 \mu\text{N}$, remains notably below the maximum driving force, $F_{dmax} \approx 5.8 \mu\text{N}$.

While we present the dissipation analysis of a representative moving droplet in Fig. 5, F_{diss} has consistently remained substantially less than F_{dmax} in all our exper-

iments. Therefore, we believe that other dissipative factors must have contributed to slowing down the droplets. Given the small capillary number of the moving droplets, $Ca = \eta_l V / \gamma_l \sim 10^{-7}$, the viscous dissipation within the droplets can be neglected [22, 26]. We speculate that the pinning from the physical boundary between two gels was a significant contributor to the difference between F_{dmax} and F_{diss} . Specifically, it is challenging to prevent interfacial deformations between cured gels with different crosslinking densities, and in this instance, the boundary served as a pinning defect and thus dissipated the force required for droplet movement [27].

V. CONCLUSIONS

In this study, we reported an experimental observation of spontaneous droplet motion on the surfaces of soft gels (Fig. 1). The movements were induced by the contact angle difference between gels with different Young's moduli (Fig. 3) but dissipated by the deformed substrates (Fig. 5). We experimentally demonstrated that increasing the gradient of crosslinking density enables a droplet to climb a tilted plane with a steeper slope (Fig. 4).

As the moving droplets were a few millimeters in size, the elastocapillary effects of the soft substrates, which were previously investigated [17], played an insignificant

role in this study (Fig. 2). We attribute the spontaneous droplet migration to the surface energy gradient that resulted from the spatially varying crosslinking densities. This conclusion is consistent with the findings of our previous study, which explored the role of crosslinking density in the surface stress and surface energy of soft gels [18]. The present study demonstrated an effective approach for controlling droplet motion on soft interfaces. In future work, it will be appealing to realize systems with a continuous gradient of crosslinking density, as such systems may prevent dissipations from boundaries between sharply changing gel matrices. Consequently, experimental studies of such systems may yield results that can be directly compared with the existing theoretical predictions [14–16].

ACKNOWLEDGMENT

We thank Caishan Yan and Chang Xu for use discussions. This study was financially supported by the General Research Funds (16305821 and 16306723), the Early Career Scheme (26309620), and the Collaborative Research Fund (C6004-22Y) from the Hong Kong Research Grants Council. We also thank the support from the Department of Science and Technology of Guangdong Province Collaborative Research Grant (2023A0505030017).

-
- [1] L. Trichet, J. L. Digabel, R. J. Hawkins, S. R. K. Vedula, M. Gupta, C. Ribault, P. Hersen, R. Voituriez, and B. Ladoux, Evidence of a large-scale mechanosensing mechanism for cellular adaptation to substrate stiffness, *Proceedings of the National Academy of Sciences* **109**, 6933 (2012).
 - [2] D. E. Discher, P. Janmey, and Y. li Wang, Tissue cells feel and respond to the stiffness of their substrate, *Science* **310**, 1139 (2005).
 - [3] P. Zhu and L. Wang, Microfluidics-enabled soft manufacture of materials with tailorable wettability, *Chemical Reviews* **122**, 7010 (2022).
 - [4] Q. Yuan and Y.-P. Zhao, Precursor film in dynamic wetting, electrowetting, and electro-elasto-capillarity, *Phys. Rev. Lett.* **104**, 246101 (2010).
 - [5] R. Lhermerout, H. Perrin, E. Rolley, B. Andreotti, and K. Davitt, A moving contact line as a rheometer for nanometric interfacial layers, *Nature Communications* **7**, 12545 (2016).
 - [6] N. Gao, F. Geyer, D. W. Pilat, S. Wooh, D. Vollmer, H.-J. Butt, and R. Berger, How drops start sliding over solid surfaces, *Nature Physics* **14**, 191 (2018).
 - [7] H. K. Khattak, S. Karpitschka, J. H. Snoeijer, and K. Dalnoki-Veress, Direct force measurement of microscopic droplets pulled along soft surfaces, *Nature Communications* **13**, 4436 (2022).
 - [8] T.-S. Wong, S. H. Kang, S. K. Y. Tang, E. J. Smythe, B. D. Hatton, A. Grinthal, and J. Aizenberg, Bioinspired self-repairing slippery surfaces with pressure-stable omniphobicity, *Nature* **477**, 443 (2011).
 - [9] M. K. Chaudhury and G. M. Whitesides, How to make water run uphill, *Science* **256**, 1539 (1992).
 - [10] A. Lafuma and D. Quéré, Superhydrophobic states, *Nature Materials* **2**, 457 (2003).
 - [11] L. Courbin, E. Denieul, E. Dressaire, M. Roper, A. Ajdari, and H. A. Stone, Imbibition by polygonal spreading on microdecorated surfaces, *Nature Materials* **6**, 661 (2007).
 - [12] M. Coux and J. M. Kolinski, Surface textures suppress viscoelastic braking on soft substrates, *Proceedings of the National Academy of Sciences* **117**, 32285 (2020).
 - [13] D. Paretkar, X. Xu, C.-Y. Hui, and A. Jagota, Flattening of a patterned compliant solid by surface stress, *Soft Matter* **10**, 4084 (2014).
 - [14] A. Bardall, S.-Y. Chen, K. E. Daniels, and M. Shearer, Gradient-induced droplet motion over soft solids, *IMA Journal of Applied Mathematics* **85**, 495 (2020).
 - [15] J. Bueno, Y. Bazilevs, R. Juanes, and H. Gomez, Wettability control of droplet durotaxis, *Soft matter* **14**, 1417 (2018).
 - [16] P. E. Theodorakis, S. A. Egorov, and A. Milchev, Stiffness-guided motion of a droplet on a solid substrate, *The Journal of Chemical Physics* **146**, 244705 (2017).
 - [17] R. W. Style, Y. Che, S. J. Park, B. M. Weon, J. H. Je, C. Hyland, G. K. German, M. P. Power, L. A. Wilen, J. S. Wettlaufer, *et al.*, Patterning droplets with durotaxis, *Proceedings of the National Academy of Sciences* **110**, 12541 (2013).

- [18] W. Zhao, J. Zhou, H. Hu, C. Xu, and Q. Xu, The role of crosslinking density in surface stress and surface energy of soft solids, *Soft Matter* **18**, 507 (2022).
- [19] Q. Xu, L. A. Wilen, K. E. Jensen, R. W. Style, and E. R. Dufresne, Viscoelastic and poroelastic relaxations of soft solid surfaces, *Phys. Rev. Lett.* **125**, 238002 (2020).
- [20] R. W. Style, R. Boltyanskiy, Y. Che, J. S. Wettlaufer, L. A. Wilen, and E. R. Dufresne, Universal deformation of soft substrates near a contact line and the direct measurement of solid surface stresses, *Phys. Rev. Lett.* **110**, 066103 (2013).
- [21] Q. Xu, K. E. Jensen, R. Boltyanskiy, R. Sarfati, R. W. Style, and E. R. Dufresne, Direct measurement of strain-dependent solid surface stress, *Nature Communications* **8**, 555 (2017).
- [22] X. Li, F. Bodziony, M. Yin, H. Marschall, R. Berger, and H.-J. Butt, Kinetic drop friction, *Nature Communications* **14**, 4571 (2023).
- [23] M. E. Shanahan and A. Garré, Viscoelastic Dissipation in Wetting and Adhesion Phenomena, *Langmuir* **11**, 1396 (1995).
- [24] S. Karpitschka, S. Das, M. van Gorcum, H. Perrin, B. Andreotti, and J. H. Snoeijer, Droplets move over viscoelastic substrates by surfing a ridge, *Nature communications* **6**, 7891 (2015).
- [25] M. Zhao, J. Dervaux, T. Narita, F. Lequeux, L. Limat, and M. Roché, Geometrical control of dissipation during the spreading of liquids on soft solids, *Proceedings of the National Academy of Sciences of the United States of America* **115**, 1748 (2018).
- [26] X. Li, P. Bista, A. Z. Stetten, H. Bonart, M. T. Schür, S. Hardt, F. Bodziony, H. Marschall, A. Saal, X. Deng, *et al.*, Spontaneous charging affects the motion of sliding drops, *Nature Physics* **18**, 713 (2022).
- [27] D. Guan, Y. J. Wang, E. Charlaix, and P. Tong, Asymmetric and speed-dependent capillary force hysteresis and relaxation of a suddenly stopped moving contact line, *Phys. Rev. Lett.* **116**, 066102 (2016).